Chapter 3

Materials and Methods

3.1 Methodology Flow Diagram

The following flowchart (**Fig 3.1**) outlines the methodology employed in this study for the conversion of raw biomass into value-added products. The process begins with the characterization and preparation of raw biomass, including cleaning, drying, grinding, and sieving, to obtain a processed biomass sample. The prepared biomass undergoes pyrolysis, a thermochemical decomposition process, accompanied by detailed kinetic and thermodynamic studies. Several ZSM-5 catalysts are introduced during pyrolysis to enhance the yield and quality of the products. The resulting pyrolysis products—biochar, bio-oil, and gas—are subjected to analysis and characterization to compare catalytic and non-catalytic pyrolysis. To further optimize the process and predict outcomes, Response Surface Methodology (RSM) and Artificial Neural Networks (ANN) are applied and compared. This systematic approach ensures a comprehensive understanding of the biomass conversion process and its performance.

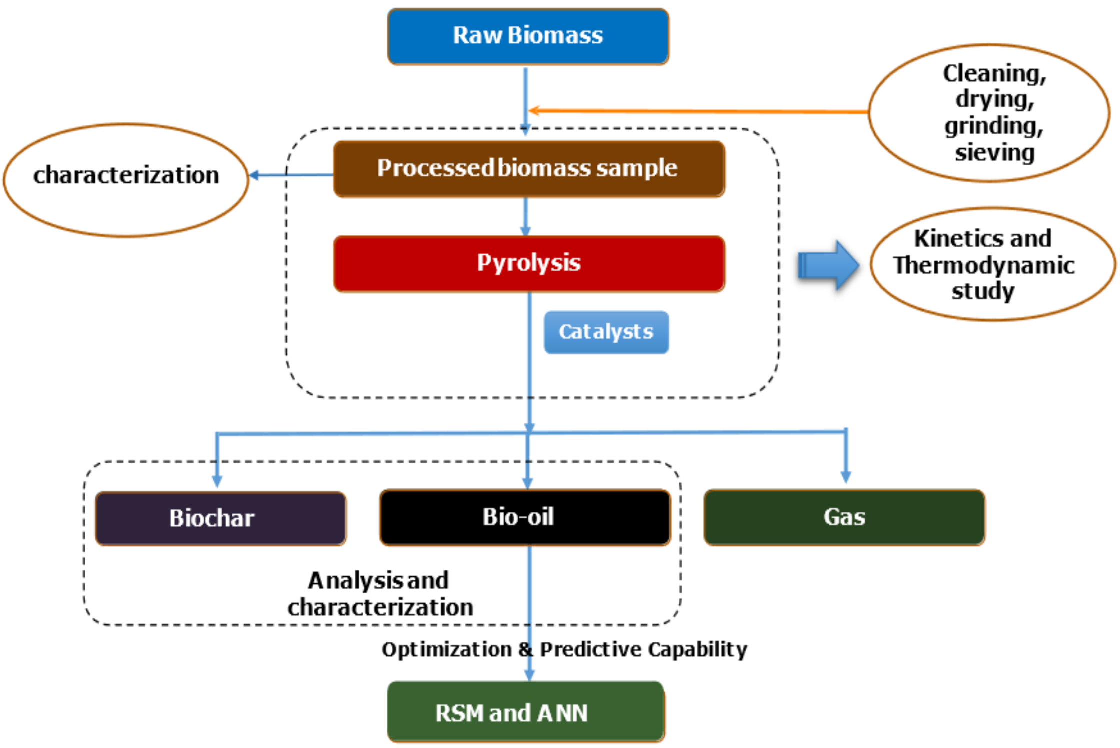

Fig. 3.1: Flow diagram of the methodology adopted for the study

3.2 Identification and Description of the Feedstock

A species of weed, *Tithonia diversifolia*, known for its invasive properties was identified and collected from the Sonitpur district in Assam, located in the north-eastern part of India. Assam lies at coordinates 26.2006° N and 92.9376° E and experiences a predominantly warm and moist climate, with the exception of some central regions. Temperature fluctuations are common, ranging from 22 °C to 35 °C in the summertime, and dropping to a cooler 10 °C to 30 °C during the winter months. High humidity levels, between 75-90%, are a constant feature across the state year-round. The state receives an annual rainfall that typically falls between 1700 and 2100 millimeters [1].

3.2.1 *Tithonia diversifolia*: The Feedstock in the Current Investigation

Fig. 3.2: *Tithonia diversifolia*

Scientific classification of the feedstock:

Species: *T. diversifolia*

Kingdom: Plantae

Family: *Asteraceae*

Genus: *Tithonia*

Tithonia diversifolia (TD), commonly referred to as Mexican sunflower or tree marigold, is a robust annual or perennial herbaceous and bushy plant with a woody base, growing to a height of about 2.5 m belongs to the family Asteraceae [2]. The stems of *Tithonia diversifolia* are cylindrical, hollow, slightly ridged, and hairy when young. The leaves, borne on stalks, are simple, alternate, and finely hairy; they have a tapered base and

3-7 pointed lobes with scalloped or toothed margins. A photograph of the species has been shown in **Fig. 3.2**. The flower heads look like sunflowers but have yellow centers. They are borne on long stalks, velvety beneath the heads, and are arranged in small groups at the ends of the branches. The fruit is a blackish hairy achene topped with a ring of scales and two awns. It can grow throughout the year and its seeds are spread through way of wind, water, and animals.

3.2.1.1 Distribution of *T. diversifolia*

This aggressive weed plant has been found on disturbed sites, abandoned farmlands, wastelands, roadsides, forest edges, field edges, riverbanks, and disturbed secondary forests at elevations ranging from near sea level to 2300 m [5, 10, 31]. It originated from Mexico and Central America and is now widely distributed throughout the tropical and subtropical regions of the world, including Central and South America, Africa, Asia, Australia, the West Indies, and many islands across the Pacific and Indian Ocean [3, 8, 31].

In India, *Tithonia diversifolia* is distributed widely across several states. In southern India, it has been recorded in Karnataka, specifically the Hassan district, and across all districts of Kerala. It is also present in Tamil Nadu (Salem and Madurai districts) and Odisha [32, 33]. In Maharashtra, the plant has been reported, along with northeastern states like Nagaland, Arunachal Pradesh, Mizoram, Manipur and Meghalaya. In Assam, it has been recorded in Bokakhat, Jorhat, and several other districts [33, 34]. This extensive spread in Assam and neighboring states highlights its adaptability to diverse environments, aided by its high seed production potential, which can reach up to 900,000 seeds/m^2 [35].

The rapid spread of *T. diversifolia* is facilitated by its tolerance to heat and drought, its rapid growth rates, and its ability to produce large quantities of small seeds that are easily dispersed by wind, water, and animals [4]. Once established, it quickly forms dense stands that out-compete native vegetation, preventing the recruitment and growth of native plant species. In addition, it may also affect the loss of medicinal resources as it contains a large amount of allelochemicals especially in leaves which inhibit the growth of many plants [5]. Furthermore, *T. diversifolia* has been reported as a weed in rice, sorghum, and maize plantations [9]. One study found that when dried leaf material comprised more than 4% of broiler feed, carcass traits and sensory characteristics were adversely affected [35]. However, despite its invasive nature, the plant has some economic and traditional uses, such as fuelwood, building materials, compost, and land demarcation [3]. The leaves of

Tithonia diversifolia are also used in traditional medicine for treating constipation, stomach pains, liver pains, indigestion, sore throats, and as an antiviral [6, 7]

3.3 Material and Analytical Test Method

3.3.1 Sample Preparation

Biomass material for the current study was gathered from nearby areas of Tezpur University, Tezpur, Assam. The entire plant excluding the roots were collected and washed thoroughly to remove extraneous particles, cut into small pieces and then sun-dried followed by oven drying for 12 h at 105 °C. After that, samples were grounded using a Wiley machine (SECOR Scientific Eng. Co) with different sieve sizes to produce samples with different particle sizes (<0.25 mm, 0.25- 0.5mm, 0.5- 0.84 mm, 0.84-1mm, and >1 mm). For the preliminary analysis, biomass particles smaller than 0.25 mm (60 mesh) were used and stored in sealed containers. To assess the impact of particle size on *Tithonia diversifolia* biomass pyrolysis, all particle sizes were evaluated.

3.3.2 Proximate Analysis

3.3.2.1 Determination of moisture content

The moisture content (MC) of the samples under investigation was determined following the ASTM D-3173 method. At first, a certain amount of the fresh sample was taken in an aluminum container and weighed by using an electronic balance. Then the sample was oven-dried at a temperature of 105±3 °C until a constant weight was obtained. For each sample, the experiment was performed in triplicate and the mean value was reported. The moisture content (MC) was calculated by using the following equation:

$$Moisture\ content\ (\%) = \frac{Initial\ weight - Oven\ dry\ weight}{Initial\ weight} \times 100 \qquad \text{.......(1)}$$

3.3.2.2 Determination of ash content

The ash content (AC) of the samples was determined by using the ASTM D-3174 method. At first, an empty 25 ml silica crucible was dried in a muffle furnace at a temperature of 575 ± 25 °C for 15 minutes and then allowed to cool in desiccators for 45 min and weighed precisely. About 2 g of the oven-dried sample was weighed and transferred to a completely dried crucible and then kept in a muffle furnace at 575 ± 25 °C for six hours until complete combustion of the sample took place as indicated by the absence of black particles. When the furnace was cooled down, the crucible was taken out, kept in a desiccator, and weighed accurately. For each sample, the experiment was done in triplicate and the mean value was reported. The percentage of ash content (AC) was determined by using the following formula:

$$Ash\ content\ (\%) = \frac{Weight\ of\ ash}{Weight\ of\ sample} \times 100 \quad \ldots\ldots(2)$$

3.3.2.3 Determination of volatile matter

The volatile matter (VM) of the samples was determined by the ASTM D-3175 method. A silica crucible with 10 ml capacity was dried in a preheated vertical tube furnace at 950 ºC for 2 min and then allowed to cool in a desiccator for 15 min. Then the weight of the empty crucible was taken. About 2 g of the oven-dried biomass sample was taken in the dried crucible, covered with a lid, and placed in the preheated vertical tube furnace at 950 ºC for about 2 minutes. Then the crucible was removed from the furnace and allowed to cool in air for 2 to 5 min and then in a desiccator for about 15 minutes. The weight loss percentage was reported as volatile matter (VM) content which was calculated as follows:

$$volatile\ matter\ (\%) = \frac{Weight\ loss\ of\ dry\ sample}{Net\ weight\ of\ dry\ sample} \times 100 \quad \ldots\ldots(3)$$

3.3.2.4 Fixed carbon

The fixed carbon content of the samples was determined by the method given in ASTM Test No. D-271-48. Fixed carbon content was calculated by subtracting the sum of percentages of moisture, ash, and volatile matter from 100.

$$Fixed\ carbon\ (dry\ basis)(\%) = 100 - [MC(\%) + VM\ (\%) + AC(\%)] \ldots\ldots(4)$$

3.3.3 Biochemical Analysis of Biomass

The biochemical components, i.e., hemicellulose, cellulose, lignin, and extractive of the biomass samples were done using the method illustrated elsewhere [11]. The methods adopted are discussed in the following subsections.

3.3.3.1 Extractives

The dried biomass sample (W_0, g) is leached with a mixture of benzene/ethanol (2:1 in volume) at a constant temperature for 3 h. After air-drying, the residue is dried in an oven at 105 –110 °C to a constant weight. Then the residue is cooled to room temperature in a desiccator and then weighed (W_1, g). The extractive wt.% is calculated as:

$$Extractives, E\ (\%) = \frac{W_0 - W_1}{W_0} \times 100 \quad ....(5)$$

3.3.3.2 Hemicellulose

The residue W_1 from the extractive analysis was placed in a flask and then added to a 150 ml NaOH solution (20 g/l). The mixture was boiled for 3.5 hours with recycled distilled water. The residue was filtered and washed until no more Na^+ ions were present, and it was subsequently dried to a constant weight. The residue is then cooled to room temperature in a desiccator and weighed (W_2, g). The hemicellulose wt.% is calculated as:

$$Hemicellulose, Hc\ (\%) = \frac{W_1 - W_2}{W_0} \times 100 \quad ....(6)$$

3.3.3.3 Lignin

Approximately 1 g of residue, from the extractives analysis outlined above, was placed into a pre-weighed flask. The residue was dried until a constant weight was achieved. Subsequently, the sample was cooled within a desiccator and weighed (W_3, g). A quantity of 30 ml of sulfuric acid (72%) was carefully poured into the sample. The mixture was maintained at a temperature between 8 and 15 °C for a duration of 24 hours. Following this period, the mixture was transferred to a flask and diluted with 300 ml of distilled water. The sample was then boiled for 1 hour using recycled distilled water. After cooling and filtration, the residue is washed until there is no more sulfate ion in the filtrate (detected by 10% barium chloride solution). The residue is then dried to a constant weight, cooled to room temperature in a desiccator, and weighed (W_4, g). The hemicellulose wt.% is calculated using the following formula:

$$Lignin, L\ (\%) = \frac{W_4(1 - Extractive,\ wt\,\%)}{W_3} \times 100 \quad ....(7)$$

3.3.3.4 Cellulose

The cellulose wt.% is calculated as:

$$Cellulose, (\%) = 100 - (AC\,\% + E\,\% + Hc\,\% + L\,\%) \quad ....(8)$$

3.3.4 Pyrolysis Experiments

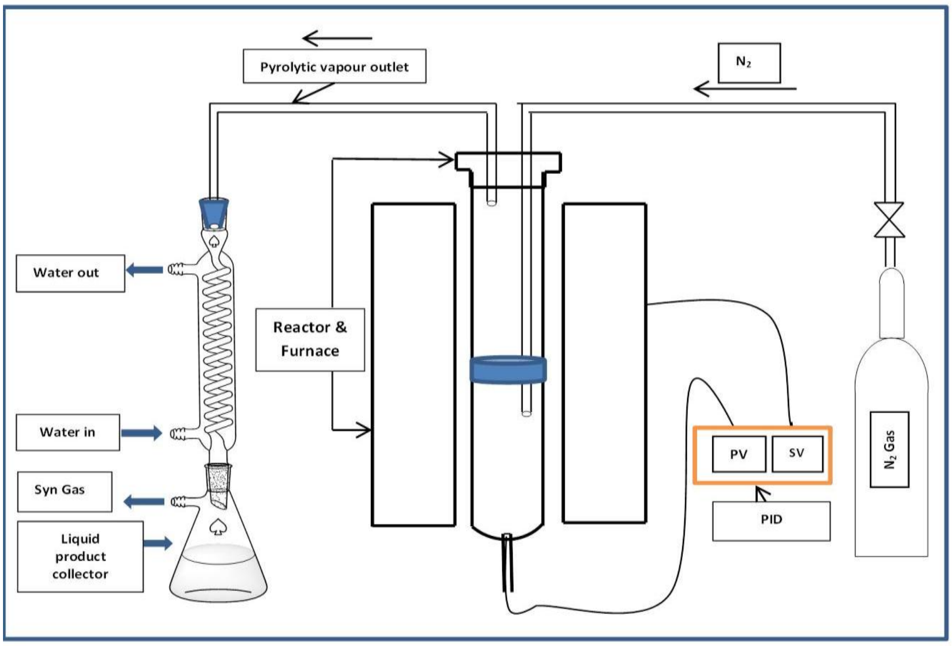

Fig. 3.3: Schematic of pyrolysis experimental setup

The thermo-chemical conversion i.e., pyrolysis experiments were conducted in a fixed-bed tubular pyrolysis reactor system (Montech Instruments, Chandigarh, India). In this system, the temperature was controlled by a Ni-Cr thermocouple placed in the center of the pyrolysis reactor as shown in **Fig 3.3**. The biomass sample (10 g) was placed in the lab-scale fixed-bed tubular reactor (length 30 cm and internal diameter 2.47 cm) made up of quartz. The bed height of the biomass in the reactor was approximately 5 cm, depending on the size of the sample particles.

The pyrolysis of the samples was performed in the reactor at different operating conditions or parameters. A condenser was attached to the outlet of the reactor to condense the vapors coming out of it. The condensed liquid was collected in a container at the end of the condenser. The liquid product consists of two phases: the aqueous phase (it is mainly composed of acids, sugars, and other highly polar organic compounds) and the organic phase (**Fig 3.4**). The organic phase was extracted with an equal quantity of diethyl ether. The obtained ether fraction (organic phase) was dried over anhydrous sodium sulfate, filtered, and evaporated in a rotary evaporator at 30 °C to remove diethyl ether. Then this fraction was weighed, bottled, and indicated as bio-oil in the present study. The liquid products and char yield were determined by weighing and the gas yield was determined by difference as mentioned in equations (9) and (10). Triplicate experiments were conducted for each sample yielding outputs with acceptable experimental margins.

$$\text{Product yield (wt. \%)} = \frac{weight\ of\ the\ product}{weight\ of\ the\ biomass\ sample} \times 100 \qquad \ldots\ldots(9)$$

$$\text{Gas Yield, (wt. \%)} = 100 - [\text{ Oil yield (wt. \%)} + \text{Biochar yield (wt. \%)}] \ldots\ldots(10)$$

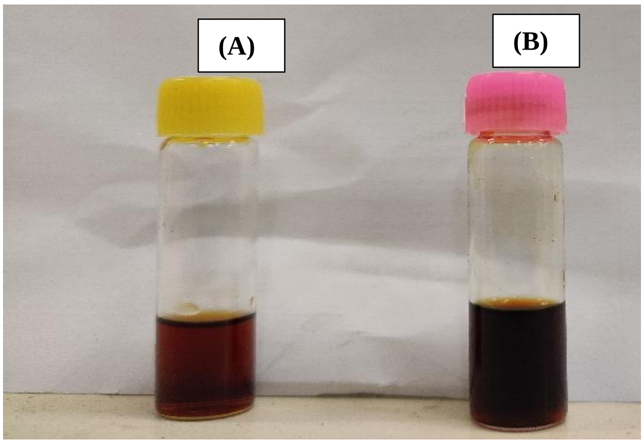

Fig. 3.4 Pyrolysis liquid product (A) Aqueous phase (B) Organic phase

3.3.4.1 Effect of operating conditions on product distribution

For estimation of the optimum operating conditions for highest products yield classically, temperature (T) from 400 – 600°C were selected along with heating rates (HR) 10, 20, 30 and 40 °C/min; nitrogen flow rates (NFR) of 50, 100, 150, 200 mL/min; and different particle sizes (PS in mm) of >0.84, 0.5-0.84, 0.25-0.5 and <0.25 mm, with holding time of 30 min.

To study the effect of operating conditions on biomass pyrolysis, experiments were conducted systematically under varying parameters. Initially, 10 g of biomass sample with a particle size (PS) of <0.25 mm was placed in the reactor. A nitrogen flow rate (NFR) of 50 mL/min was initiated to ensure an inert atmosphere and maintained throughout the pyrolysis process. The feedstock was subjected to heat treatment at a constant heating rate (HR) of 10 °C/min, with final temperatures of 400, 450, 500, 550, and 600 °C. After pyrolysis, the liquid products and solid residue were collected and weighed to determine product yields.

In the second set of experiments, the effect of HR on bio-oil yield was evaluated by varying the HR at 10, 20, 30, and 40 °C/min while maintaining the optimal pyrolysis temperature (determined in the first step). The biomass PS (<0.25 mm) and NFR (50 mL/min) were kept constant.

Subsequently, the impact of PS was studied by keeping the optimal temperature and HR constant. Biomass samples with particle sizes of >0.84 mm, 0.5–0.84 mm, 0.25–0.5 mm, and <0.25 mm were tested at NFR of 50 mL/min.

Finally, the effect of NFR on product yield was investigated while maintaining the optimal parameters for temperature, HR, and PS. The NFR was varied at 50, 100, 150, and 200 mL/min, and the flow rate corresponding to the maximum bio-oil yield was identified.

3.3.5 Statistical Modelling

3.3.5.1 Response surface methodology

To predict the output response of a particular problem due to the interaction of various input factors; Box and Wilson derived a regression method in 1951 which facilitated exploring the association among the factors and their response [12]. To increase or forecast the highest yield of bio-oil from the above-mentioned biomass, the pyrolysis experiment was developed with the design expert software (Version 10.0.6, Stat- Ease Inc., MN, USA) using CCD-based response surface methodology (RSM). CCD was used due to a smaller number of experiments and the use of a second-order model fitting for the prediction and verification of the model equation. The four independent parameters to obtain a realistic model are; temperature (T °C); heating rate (HR °C/min); nitrogen flow rate (FR mL/min) and particle size (PS mm). The parameters were coded as A, B, C, and D respectively. Bio-oil yield (Y_{BO}) was taken as a response for the experiments.

Table 3.1 represents the levels of the independent variables (coded and uncoded) whereas **Table 3.2** depicts the CCD for the experiment. The general form for second-order polynomial equation is shown below:

$$Y_{BO}= \alpha_0 + \sum_{i=1}^{n} \alpha_i Z_i + \sum_{i=1}^{n} \alpha_{ii} XZ_i^2 + \sum_{i}^{n} \sum_{j>1}^{n} \alpha_{ij} Z_i Z_j \qquad (11)$$

Where, Y_{BO}= predicted bio-oil yield, n = number of tests, α_o, α_i, α_{ii}, α_{ij}were the constant, linear, quadratic, and interaction coefficients respectively and X_i and X_j were coded independent factors.

Table 3.1: Process parameters and their levels

Coded factors	Factors	Experimental Levels				
		- α	**-1**	**0**	**+1**	**+ α**
A	**Temperature (°C)**	375	450	525	600	675
B	**Heating rate (°C/min)**	10	20	30	40	50
C	**Flow rate (mL/min)**	50	100	150	200	250
D	**Particle size (mm)**	0.25	0.5	0.75	1	1.25

In this study, the particle size was set in five categories, which are 0.25 <PS~0.25 mm, 0.25 <PS< 0.5~0.5 mm, 0.5 <PS< 0.84~0.75 mm, 0.84<PS<1mm~1mm and PS> 1~1.25 mm.

Graphical and numerical representations were carried out along with an analysis of variance (ANOVA) to test the statistical significance of the regression coefficient. Based on P<0.05, the significance of model terms was judged. Finally, the model fitness was measured by calculating the “lack-of-fit”. Based on the effect of the four parameters, three-dimensional response surface plots were derived which is also used to study the interaction effect. In addition to that optimum process conditions for maximum bio-oil yield were also evaluated using a design expert tool.

Table 3.2: CCD experimental design matrix

Sl No.	Temperature (°C)	Heating rate (°C/min)	Flow rate (mL/min)	Particle size (mm)
1	450	20	200	1
2	375	30	150	0.75
3	450	40	100	0.5
4	525	30	150	0.75
5	600	40	100	0.5
6	525	30	150	1.25
7	675	30	150	0.75
8	450	40	200	0.5
9	525	30	150	0.75
10	600	40	100	1
11	600	20	200	0.5
12	600	20	100	1
13	450	20	100	0.5
14	600	20	200	1
15	525	30	150	0.75
16	450	20	200	0.5
17	450	20	100	1
18	525	30	150	0.75
19	600	40	200	1
20	525	10	150	0.75
21	450	40	200	1
22	525	30	250	0.75
23	525	30	50	0.75
24	450	40	100	1
25	525	50	150	0.75
26	525	30	150	0.25
27	525	30	150	0.75
28	600	20	100	0.5
29	600	40	200	0.5
30	525	30	150	0.75

3.3.5.2 ANN modelling

An artificial neural network (ANN) is a promising alternative modeling technique inspired by biological neural systems [13]. It consists of a large number of neurons or processing elements or units in different layers that are interconnected to one another through weights. Through adjusting connecting weights, bias, and architecture; neurons are trained to perform a particular task [14]. The network architecture of neural networks was determined by how artificial neurons were mutually connected, and more than fifty types of network architecture could be found in the literature [15]. The systems showing nonlinearities and complex behavior can be well predicted using neural networks due to their ability to learn from a set of experimental data (e.g., process conditions and responses) with minimal prior knowledge about their further properties and mechanisms.

A feedforward or backpropagation network is a widely used neural network consisting of several inputs and one output in each processing element [15]. A multilayer perceptron (MLP) is a feedforward ANN that is comprised of three or more layers of neurons. Independent input variables from the first layer of neurons (i.e., input layer) are connected to neurons of hidden layers. Propagation of the data from the input layer to the first hidden layer within the network occurred via the connections and the associated activation functions combined and modified those. Each layer has a certain number of neurons with corresponding weight and bias; and the ANN model for a particular task was dependent upon the nature of these connections, which provides additional adjustable parameters. In this way, the signals were propagated through each layer until they reached the output layer. The impact of each input neuron and its complex interactions can be identified by employing learning algorithms. Optimized ANNs are capable of approximating any continuous non-linear function, being highly resistant to missing or noisy data [13].

3.3.5.2.1 Topology

The most important part of selecting an ANN model for the prediction of experimental data is the topology and the architecture of the neural network [16]. The topology of an ANN is determined by the number of layers in the ANN, the number of nodes in each layer, and the nature of the transfer functions. Levenberg-Marquardt (LM) algorithm was used for modelling the process parameters of the pyrolysis process in multi-layer perception (MLP) neural network analysis. The neural network toolbox (nntool) of

MATLAB 2016a (9.0.0.341360) was used in this modelling. The feedforward network needs outputs to train the model. A representation of the ANN architecture is shown in **Fig. 3.5** with four variables viz. T, HR, FR, and PS in the input layer followed by one hidden and output layer, i.e., bio-oil yield. In this investigation, a hyperbolic tangent sigmoid function (tansig) transfer function was used in the hidden layer whilst a linear transfer function (purelin) was used in the output layer. To assess the robustness of the prediction ability of the models, a total of 30 experimental results generated in CCD design were employed to train, test, and validate the model. Out of these, 70% were used for network training, and the rest 30% were fragmented between testing and validation of the network. TRAINLM function is employed for training models which is the fastest back-propagation algorithm. Gradient descent learning function (LEARNGD) was used to minimize the errors. All training parameters of the ANN are shown in **Table 3.3**. The optimum hidden neurons number was set based on the lowest output data obtained for MSE, and one hidden layer of fourteen neurons is considered the best result. The total number of iterations for ANN training was set as 100,000 while the other parameters were kept as the preset input of the software.

Table 3.3: ANN parameters used to train, model, and optimize the bio-oil yield

Particulars	**Specifications**
Network type	Feed-forward back-propagation
Training function or training algorithm	Levenberg-Marquardt backpropagation (TRAINLM)
Adaptation learning function	Gradient descent (LEARNGD)
Performance function	Mean Square Error (MSE)
Transfer function	Hyperbolic Tangent Sigmoid (TANSIG)
Output layer	PURELIN
Number of input layer	4
Number of output layer	1
Number of hidden layer	1
Number of hidden layer neuron	14

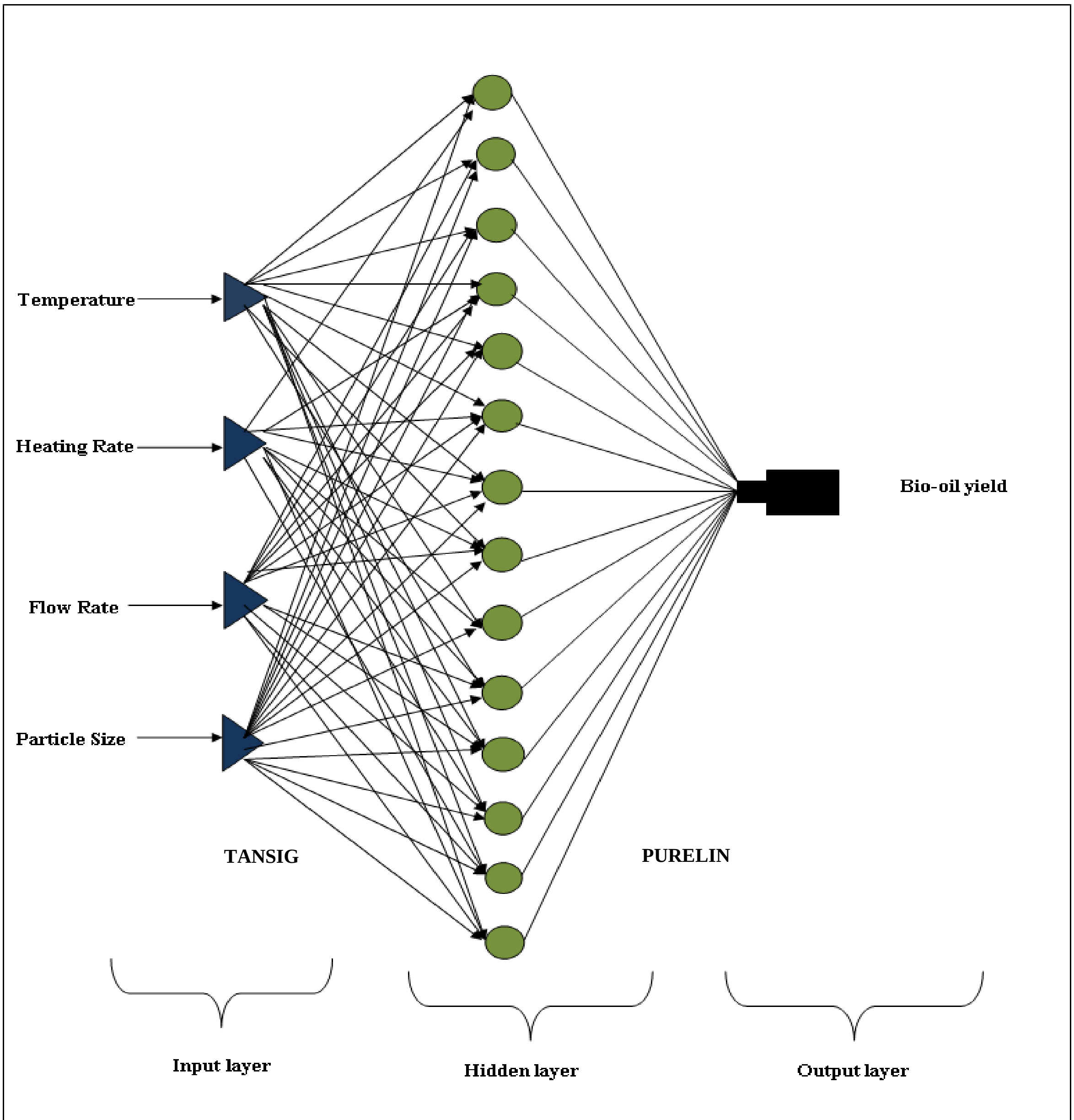

Fig. 3.5 ANN architecture

3.3.5.3 Prediction capability of the RSM and ANN models

The coefficient of determination (R^2), root mean square error (RMSE), mean absolute error (MAE), absolute average deviation (AAD), and standard error of prediction (SEP) was used for statistical assessment of the prediction ability of the models developed by using RSM and ANN. These are evaluated according to equations (12) to (16) [17].

The amount of reduced response variability in the model is measured by R^2 while AAD deals with the deviations. The precision of the model is determined by evaluating R^2 and AAD values. R^2 must be close to “1” and the smaller the AAD value, the more precise the model is [18]. The acceptable values of R^2 and AAD values mean that the model equation determines the system's true behaviour and it can be used for interpolation in the experimental domain [19].

$$R^2 = 1 - \frac{\sum_{i=1}^{n}\left(x_{e,i} - x_{p,i}\right)^2}{\sum_{i=1}^{n}\left(x_{p,i} - x_{e.ave}\right)^2} \qquad (12)$$

$$RMSE = \sqrt{\frac{1}{n}\sum_{i=1}^{n}\left(x_{p,i} - x_{e,i}\right)^2} \qquad (13)$$

$$MAE = \frac{1}{n}\sum_{i=1}^{n}\left|\left(x_{e,i} - x_{p,i}\right)\right| \qquad (14)$$

$$SEP = \frac{RMSE}{x_{e.ave}} \times 100 \qquad (15)$$

$$AAD = \frac{100}{n}\sum_{i=1}^{n}\left|\frac{x_{e,i} - x_{p,i}}{x_{e,i}}\right| \qquad (16)$$

where n is the number of experiments, $x_{e,i}$ is the experimental results, $x_{p,i}$ is the predicted outputs, and $x_{e,ave}$ is the average experimental results.

3.3.5.4 Application of catalysts in biomass pyrolysis

3.3.5.4.1 Preparation of catalysts

ZSM-5 (Alfa Aesar, molar ratio of 50:1) zeolite was calcined at 550 °C for 5 hr at a heating rate of 5°C/min, for transformation to its protonic form [29]**.** The obtained HZSM-5 was employed to form Ni/ZSM-5 and Co/ZSM-5 catalysts with 1 wt% metal by wet impregnation. To achieve this, equimolar amounts of 1 wt% nickel nitrate, $Ni(NO_3)_2{\cdot}6H_2O$ (Sigma-Aldrich) and cobalt nitrate, $Co(NO_3)_2{\cdot}6H_2O$ (Sigma-Aldrich), were dissolved separately in water. Then ZSM-5 was introduced into the corresponding metal nitrate solution, with continuous stirring at 80 °C for 3 hours [28]. Following that, the slurry was subjected to drying at 100 °C for 24 hours and calcined at 500 °C for 4 hr at 5 °C/min to achieve uniform distribution on both the internal and external catalyst surfaces, leading to the creation of the respective metal oxides. The zeolites that underwent post-treatment were labeled as M/ZSM-5, with 'M' representing the metal oxide that was loaded. Prior to the experiment, prepared catalysts were stored in a desiccator to prevent moisture.

3.3.5.4.2 Catalytic pyrolysis

The effect of the catalysts in pyrolysis was investigated at the biomass-to-catalyst ratio of 10:1, and each experiment was operated at 500 °C, HR of 40 °C/min, with a residence time (RT) of 30 min. The temperature of 500 °C and the heating rate of 40 °C/min were selected based on preliminary pyrolysis experiments conducted to evaluate the effect of operating parameters on product distribution. These experiments indicated that the selected conditions resulted in the highest bio-oil yield during non-catalytic pyrolysis.

For the catalytic pyrolysis experiments, both the biomass and catalyst were ground to a particle size of <0.25 mm to ensure uniform mixing and maximize contact between the catalyst and the biomass during the pyrolysis process. The mixture was then homogenized using a mortar and pestle followed by mixing in a cylindrical plastic container to ensure uniform distribution of the catalyst particles throughout the biomass. This facilitated smooth heat transfer and consistent catalytic activity throughout the reaction.

3.3.6 Instrumental Characterization

3.3.6.1 Elemental characterization

The elemental composition of the material was determined by the ultimate analysis. The carbon, hydrogen, and nitrogen content of the biomass samples was determined using a CHN elemental analyzer (Perkin Elmer, 2400 Series 2, USA.). The percentage of oxygen was calculated by difference.

3.3.6.2 Higher heating value (HHV)

Calorific value is the amount of heat generated when a unit weight (1 g or 1 kg) of material is burnt or combusted. It was determined by using a bomb calorimeter (Auto bomb calorimeter, SE-1AC/ML, MS. CHANGSHA KAIYUAN INSTRUMENTS CO. LTD., CHANGSHA, CHINA) according to the ASTM D2015 method. Here, about 1.0 g of finely ground oven-dried sample was pressed into a tablet with a mechanical pelletizer. Then the sample was completely combusted in an adiabatic bomb containing 3.4 MPa pure oxygen under pressure. The test was conducted in triplicates and the mean value was reported.

3.3.6.3 FTIR analysis

The presence of different functional groups in the samples was investigated by FTIR (Fourier transforms infrared spectroscopy) spectroscopy. Samples were prepared using the potassium bromide (KBr) disk technique The FTIR spectrum of the samples was recorded on a IR spectrometer (Perkin Elmer, SPECTRUM 100, USA) at room temperature (26 ± 2 °C) in the mid-infrared region of 4000-400 cm^{-1} with resolution of 4 cm^{-1}.

3.3.6.4 ^{1}H-NMR

The ^{1}H-NMR spectra of the bio-oil samples were recorded in a 400 MHz NMR spectrophotometer (JEOL, ECS 400, Japan) where deuterated chloroform ($CDCl_3$) was used as the internal standard. The coupling constants were expressed in Hertz (Hz).

3.3.6.5 GC-MS

GC–MS analysis of the bio-oil samples was carried out using a GC-MS instrument (Perkin Elmer Claurus 600, USA) equipped with a TCD detector and DB-5ms column (60.0 × 250 µm). Helium (99.99 %) with a constant flow of 1.0 ml/min was used as the carrier gas. The column temperature was programmed from 70 °C for 2 min to 290 °C at the heating rate of 10 °C min^{-1} and finally held at 290 °C for 7 min. A sample volume of 3 µL was injected. The MS was operated in an electron ionization mode and an m/z range from 24 to 624 was scanned. Peaks were identified based on the NIST library.

In the GC-MS spectra of the bio-oils, components constituting less than 0.5 Area % were disregarded and the compounds identified were classified under the following classes: phenols, alcohols, aldehydes, esters, ethers, furan, ketones, aliphatic and aromatic hydrocarbons, etc. for better comparison of bio-oils obtained from catalytic and non-catalytic pyrolysis.

3.3.6.6 Determination of pH

The pH of both bio-oil and biochar are evaluated. The pH of biochar was calculated by following the method described by Kim et al. [30]. 10 g biochar was added to 200 ml deionized water and allowed to stir for 24 hours at 180 rpm. The mixture was then filtered through Whatman 40 filter paper and the supernatant was used to measure pH by a digital pH meter (Eutech pH 700, USA). The measurement of pH helps to understand the influence of biochar application on soil acidity.

3.3.6.7 Electrical conductivity

The electrical conductivity (EC) of biochar was measured with a conductivity meter (Systronics digital TDS/conductivity meter MK509, Gujarat, India) using the same solution as prepared for pH measurement. EC values of biochar are significant as it is directly proportional to the amount of salt (ion) concentration present in biochar and is therefore, related to the buffering capacity and cation exchange capacity (CEC) of biochar.

3.3.6.8 SEM

To examine surface morphology and elemental composition of solid samples, scanning electron microscopy (JEOL JSM-6390 LV, Japan) coupled with energy dispersive X-ray spectroscopy (Oxford EDX) was used. SEM images were taken with an acceleration voltage of 20 kV at different magnifications with a resolution of 0.03 nm. The EDX is helpful in providing rapid qualitative and semi-quantitative analysis of elemental composition with a sampling depth of 1-2 microns.

3.3.6.9 XRD analysis

X-ray diffraction (XRD) analysis (D8 Focus, Bruker AXS, Germany) was conducted to assess the structure of catalysts (pre- and post-impregnation of metal into ZSM-5). The powder X-ray was recorded on a Rigaku miniflex diffractometer (Cu-Kα radiation, λ= 1.5406 Å) in 2θ range of 5-60° at a scanning rate of 20° min^{-1}.

3.3.6.10 Surface area analysis of catalysts

All the prepared catalysts were characterized for surface area, pore size, and pore volume using Quantachrome Instruments (Anton Paar, Nova 1000 E, USA). The samples underwent a degassing process of 5 hours at 150°C before the analysis. Subsequently, the samples were cooled to 77 K by immersing them in liquid nitrogen for characterization. The nitrogen adsorption method at -196 °C for analysis of the surface area. The physisorption data was utilized for the estimation of the surface area of each sample through the Brunauer-Emmett-Teller (BET) method. Furthermore, the pore distributions have been assessed by employing the Barrett-Joyner-Halenda (BJH) method.

3.3.7 Thermogravimetric Analysis (TGA)

The thermal degradation characteristics of all four specimens, i.e., TD, TD+HZSM-5, TD+Co/ZSM-5, and TD+Ni/ZSM-5, were examined using a TG analyzer (Mettler Toledo TGA/SDTA 851, Switzerland). For experiments conducted without the catalyst (TD only), approximately 5-10 mg of pure biomass (TD) was introduced directly into the alumina crucible for thermal analysis. For experiments involving catalysts, the biomass (TD) and catalyst were physically mixed in a 10:1 mass ratio. For example, if the sample contained 10 mg of biomass, 1 mg of catalyst was added and thoroughly mixed. About 5-10 mg of this prepared mixture was introduced into the alumina crucible for analysis. The mixing was conducted properly as mentioned in section 3.3.5.4.2, to ensure uniform distribution of the catalyst within the biomass prior to thermal degradation experiments. For both types of samples (Catalytic and non-catalytic), the heating process involved raising the temperature from 30 to 900 °C using three distinct heating rates – HR (10, 20, and 40 °C/min) with a gas flow rate of 50 mL min^{-1}. To ensure precision and accuracy: the TG balance had a precision of 0.1 μg and sensitivity of 0.001% and the balance accuracy was better than 0.02%. Additionally, to lessen investigational errors during the recording of thermal curves, proposals given by the Kinetics Committee of the International Confederation for Thermal Analysis and Calorimetry (ICTAC) and some other literature were followed [20-22].

3.4 Kinetic Study

The thermogravimetric information obtained at different heating rates for the samples was investigated by using Microsoft Excel 2010 and SCILAB (version 6.1.0, Windows 64 bits). The exploratory data were recorded each 0.5s time gap and the entire dataset was processed for determinations of kinetics and mechanisms of thermal degradation in the fractional conversion range of 0.025-0.900 with step size of 0.025.

3.4.1 Determination of Kinetic Parameters

During pyrolysis, the single-step thermal decomposition of biomass can be stated by the reaction scheme mentioned below:

$$Biomass \xrightarrow{\Delta} (Volatile + Gas) + Char \qquad \ldots\ldots(17)$$

The kinetic equation based on Arrhenius law for the above-mentioned reaction scheme can be written as:

$$\frac{d\alpha}{dT} = \frac{A}{\beta}\exp\left(\frac{-E}{RT}\right)f(\alpha) \qquad (18)$$

Here, E and A are respectively the activation energy in $kJ.mol^{-1}$, and Arrhenius constant in s^{-1} of the pyrolysis process, β is the heating rate in $K.s^{-1}$, T is the temperature in Kelvin, R is gas constant, 8.314 $J.mol^{-1}.K^{-1}$ and $f(\alpha)$ is the mechanism model of the decomposition process and depends on the fractional conversion, α, which can be expressed as-

$$\alpha = \frac{w_o - w_T}{w_o - w_f} \qquad (19)$$

Where, w_o, w_t, and w_f are the mass (in mg) of biomass samples at the initial temperature, T_o, at any temperature, T, and final temperature, T_f respectively.

Isoconversion methods are generally considered the best to evaluate the one-step thermal decomposition scheme without prior knowledge of the mechanism function, *f(α)* of the decomposition procedure, for the calculation of the apparent kinetics parameters [23]. Both, differential and integral isoconversional methods were used in this study to calculate the apparent activation energies of the sample. Further Miura-Maki distributed activation energy model was used for the evaluation of the apparent frequency factor values. All of the methods used in this investigation were discussed with equations in the following:

3.4.1.1 Friedman method [24]

In this differential method, the value of apparent activation energy (E_α) for a particular fractional conversion (α) value is obtained from the equation (20):

$$\ln[(\beta\frac{d\alpha}{dt})]_{\alpha,i} = \ln[A_\alpha f(\alpha)] - \frac{E_\alpha}{RT_\alpha} \qquad (20)$$

where T_α and A_α are the absolute temperature and pre-exponential factor at a given value of α, and *f*(α) is a function referring to different differential forms of reaction models. The value of E_α can be determined from the slope of the straight line obtained by plotting $\ln[(\beta\frac{d\alpha}{dT})]_{\alpha,i}$ against $1/T_\alpha$ at various heating rates.

3.4.1.2 Kissinger-Akahira-Sunose method [25]

In the Kissinger-Akahira-Sunose method, the following equation is used to determine the value of E_α:

$$(\ln\frac{\beta}{T_\alpha^2})_{\alpha,i} = \ln(\frac{A_\alpha R}{E_\alpha g(\alpha)}) - \frac{E_\alpha}{RT_\alpha} \qquad (21)$$

Where *g*(α) is a function that defines different integral forms of reaction models. The value of E_α can be determined from the slope of the plot of $(\ln\frac{\beta}{T_\alpha^2})_{\alpha,i}$ *versus* $1/T_\alpha$.

3.4.1.3 Flynn-Wall-Ozawa method [26]

This method can be used to determine the apparent activation energy (E_α) from the slope obtained from the equation (22) on plotting $(\ln\beta)_i$ against $1/T_\alpha$:

$$(\ln\beta)_i = \ln(\frac{A_\alpha E_\alpha}{Rg(\alpha)}) - 5.331 - 1.052\frac{E_\alpha}{RT_\alpha} \qquad (22)$$

3.4.1.4 Miura-Maki distributed activation energy method [27]

This method uses the same temperature integral approximation as in the KAS method, and hence the values of E_α obtained in this method are similar to those obtained in the KAS method. The advantage of this method is that the apparent Arrhenius constants (A_α) can be determined without considering the *g(α)* function. The following equation (23) is used to evaluate the values of E_α and A_α:

$$(\ln\frac{\beta}{T_\alpha^2})_{\alpha,i} = \ln(\frac{A_\alpha R}{E_\alpha}) - 0.6075 - \frac{E_\alpha}{RT_\alpha} \qquad (23)$$

Thus, the plot of $(\ln\frac{\beta}{T_\alpha^2})_{\alpha,i}$ *vs* $1/T_\alpha$ gives a straight line, and the slope and intercept of the line give the E_α and A_α parameters for a particular fractional conversion (α).

3.4.2 Derivation of degradation mechanisms

The $Y(\alpha)$-master plot method was used to determine the biomass degradation model where the function Y(α) is defined as:

$$Y(\alpha) = \beta_j \cdot (\frac{d\alpha}{dT})_{\alpha,j} \cdot \exp\left(\frac{E_o}{RT_{\alpha,j}}\right) = Af(\alpha) \qquad (24)$$

here, β_j is the j^{th} heating rate, E_o is the average energy determined by the Friedman method, R is the gas constant, and $T_{\alpha,j}$ is the absolute temperature for a particular α value and at the j^{th} heating rate, $(\frac{d\alpha}{dT})_{\alpha,j}$ is differential conversion to temperature at the j^{th} heating rate.

The experimental *Y(α)* was determined by putting numerical values of β_j, $(\frac{d\alpha}{dT})_{\alpha,j}, Eo, R,$ and $T_{\alpha,j}$ into equation (24). Similarly, theoretical *Y(α)* was determined by using various theoretical *f(α)* functions. Differential and integral forms (*f(α) and g(α) respectively)* of these functions used in this investigation and their physical interpretations are presented in **Table 3.4**. In the eqn. (24), A is an unknown quantity, which is removed by dividing experimental and theoretical $Y(\alpha)$ functions by *Y(0.5),* where *Y(0.5)* is the numerical value of *Y* for the conversion at $\alpha = 0.5$. The most suitable degradation process was then evaluated by plotting experimental and theoretical *Y(α)* values as a function of fractional conversion (α).

3.4.3 Determination of arrhenius constant

The Vyazovkin and Lesnikovich method was used to determine the Arrhenius constant of the thermal degradation reaction [21]. To determine the Arrhenius constant (A_α) at various fractional conversions the most suitable solid degradation model (obtained from

Y(α) master plot) and the corresponding apparent activation energies were used as shown in Eq. (25):

$$\ln A\alpha = b + aE\alpha \qquad (25)$$

where a and b are the correlation parameters and linear regression was used to calculate their values.

Table 3.4. Algebraic expressions for the *f*(α) and *g*(α) functions.

Mechanism	*Differential form, f*(α)	*Integral form, g*(α)
Nucleation models		
Power law (P2)	$2\alpha^{1/2}$	$\alpha^{1/2}$
Power law (P3)	$3\alpha^{2/3}$	$\alpha^{1/3}$
Power law (P4)	$4\alpha^{3/4}$	$\alpha^{1/4}$
Avarami-Erofe'ev (A2)	$2(1-\alpha)[-\ln(1-\alpha)]^{1/2}$	$[-\ln(1-\alpha)]^{1/2}$
Avarami-Erofe'ev (A3)	$3(1-\alpha)[-\ln(1-\alpha)]^{2/3}$	$[-\ln(1-\alpha)]^{1/3}$
Avarami-Erofe'ev (A4)	$4(1-\alpha)[-\ln(1-\alpha)]^{3/4}$	$[-\ln(1-\alpha)]^{1/4}$
Prout-Tompkins (B1)	$\alpha(1-\alpha)$	$\ln[\alpha/(1-\alpha)] + c^{\#}$
Geometrical contraction models		
Contracting area (R2)	$2(1-\alpha)^{1/2}$	$[1-(1-\alpha)^{1/2}]$
Contracting volume (R3)	$3(1-\alpha)^{2/3}$	$[1-(1-\alpha)^{1/3}]$
Diffusion models		
One-dimensional diffusion (D1)	$1/(2\alpha)$	α^2
Two-dimensional diffusion (D2)	$-[\ln(1-\alpha)^{-1}]$	$[(1-\alpha)\ln(1-\alpha)]+\alpha$
Three- dimensional diffusion (D3)	$[3(1-\alpha)^{2/3}]/[2(1-(1-\alpha)^{1/3})]$	$[1-(1-\alpha)^{1/3}]^2$
Ginstling-Brounshtein's equation (D4)	$3/[2\{(1-\alpha)^{-1/3}-1\}]$	$1-(2\alpha/3)-(1-\alpha)^{2/3}$
Reaction-order models		
Zero order (F0/R1)	1	α
First-order (F1)	$(1-\alpha)$	$-\ln(1-\alpha)$
Second-order (F2)	$(1-\alpha)^2$	$(1-\alpha)^{-1}-1$
Third-order (F3)	$(1-\alpha)^3$	$(1/2)[(1-\alpha)^{-2}-1]$
Pseudo n-th order (Fn)	$(1-\alpha)^n$	$1/(n-1)[(1-\alpha)^{1-n}-1]$

$^{\#}$ Integration constant

3.4.4 Sestak-Berggren Combined Kinetic Model

Sestak-Berggren combined autocatalytic kinetic model (CK model) is a three parameters model and can be described by using the following equation:

$$f(\alpha) = (1-\alpha)^{n}\alpha^{m}[-\ln(1-\alpha)]^{p} \tag{29}$$

Here, the terms, n, m, and p are the unknown parameters, which give information regarding the decomposition process. Thus, the equation for the CK model can be written as:

$$\frac{d\alpha}{dT} = \frac{A}{\beta}\exp\left(\frac{-E}{RT}\right)(1-\alpha)^{n}\alpha^{m}[-\ln(1-\alpha)]^{p} \tag{30}$$

The logarithmic linear form of the eqn. (30) can be represented as:

$$\ln\left\{\frac{\frac{d\alpha}{dT}}{\beta(1-\alpha)^{n}\alpha^{m}[-\ln(1-\alpha)]^{p}}\right\} = \ln A - \frac{E}{RT} \tag{31}$$

The linear regression of the left-hand side of the above equation with respect to $-\frac{1}{T}$ gives a straight line. The activation energy (*E*) and Arrhenius constant (*A*) of the thermal decomposition process of biomass for combined heating rates can be determined from the slope and intercept of the straight line, respectively. The parameters, n, m, and p can be calculated by maximizing the Pearson's ratio of linear regression to 1.

3.4.5 Determination of Thermodynamic Parameters

The changes in enthalpy (ΔH), free energy (ΔG), and entropy (ΔS) were determined by using the following equations:

$$\Delta H = E - RT \tag{26}$$

$$\Delta G = E + RT_{m}\ln\left(\frac{K_{B}T_{m}}{hA}\right) \tag{27}$$

$$\Delta S = \frac{\Delta H - \Delta G}{T_{m}} \tag{28}$$

Here, K_B is the Boltzmann constant, h is Plank's constant, and T_m is the temperature for the maximum weight loss rate.

References

1. Singh, M. K., Mahapatra, S., and Atreya, S. K. Development of bio-climatic zones in north-east India. *Energy and buildings*, 39(12):1250-1257, 2007.
2. Agbede, T. M., and Afolabi, L. A. Soil fertility improvement potentials of Mexican sunflower (*Tithonia diversifolia*) and Siam weed (*Chromolaena odorata*) using okra as test crop. *Archives of Applied Science Research*, 6(2): 42-47, 2014.
3. Van Sao, N., Mui, N.T. and Van Binh, D. Biomass production of Tithonia diversifolia (Wild Sunflower), soil improvement on sloping land and use as high protein foliage for feeding goats. *Livestock Research for Rural Development*, *22*(8), 2010.
4. Muoghalu, J.I. Growth, reproduction and resource allocation of *Tithonia diversifolia* and *Tithonia rotundifolia*. *Weed Research*, *48*(2):157-162, 2008.
5. Oluwafemi, A.B. and Olumide, A.T. Study on the effects of fresh shoot biomass of Tithonia diversifolia on the germination, growth and yield of cowpea (*Vigna unguiculata* L.). *American Journal of Experimental Agriculture*, *3*(4): 1005-1011, 2013.
6. Cos, P., Hermans, N., De Bruyne, T., Apers, S., Sindambiwe, J.B., Witvrouw, M., De Clercq, E., Berghe, D.V., Pieters, L. and Vlietinck, A.J. Antiviral activity of Rwandan medicinal plants against human immunodeficiency virus type-1 (HIV-1). *Phytomedicine*, *9*(1): 62-68, 2002.
7. Chiang, L.C., Cheng, H.Y., Chen, C.C. and Lin, C.C., In vitro anti-leukemic and antiviral activities of traditionally used medicinal plants in Taiwan. *The American journal of Chinese medicine*, *32*(05): 695-704, 2004.
8. Aboyeji, C.M., Adekiya, A.O., Dunsin, O., Agbaje, G.O., Olugbemi, O., Okoh, H.O. and Olofintoye, T.A.J., 2019. Growth, yield and vitamin C content of radish (*Raphanus sativus L.*) as affected by green biomass of *Parkia biglobosa* and *Tithonia diversifolia*. *Agroforestry Systems*, *93*: 803-812, 2019.
9. Imeokpara, P.O. and Okusanya, B.A. Relative effectiveness economics of cultural and chemical weed control methods in low land rice (Oryza sativa) in southern guinea savanna of nigeria. *Nigerian Journal of Weed Science*, *10*: 35-47, 1994.
10. Chukwuka, K.S., Ogunyemi, S., Osho, J.S.A., Atiri, G.I. and Moughalu, J.I. Eco-physiological responses of *Tithonia diversifolia* (Hemsl.) A. Gray in nursery and field conditions, *Journal of Biological Sciences*, 7(5): 771-775, 2007.

11. Li, S., Xu, S., Liu, S., Yang, C., and Lu, Q. Fast pyrolysis of biomass in free-fall reactor for hydrogen-rich gas. *Fuel Processing Technology*, *85*(8-10): 1201-1211, 2004.
12. Clark, C., and Williges, R.C. Response surface methodology central-composite design modifications for human performance research. *Human Factors*, 15(4): 295-310, 1973.
13. Muravyev, N.V. and Pivkina, A.N. New concept of thermokinetic analysis with artificial neural networks. *Thermochimica Acta*, *637*: 69-73, 2016.
14. Garson, G.D. Interpreting neural-network connection weights. *AI expert*, *6*(4): 46-51.
15. Carsky, M., and Kuwornoo, D.K. Neural network modelling of coal pyrolysis. *Fuel* 80(7): 1021-1027, 2001.
16. Maran, J.P., and Priya, B. Modeling of ultrasound assisted intensification of biodiesel production from neem (*Azadirachta indica*) oil using response surface methodology and artificial neural network, *Fuel, 143*: 262–267, 2015.
17. Samuel, O.D. and Okwu, M.O. Comparison of response surface methodology (RSM) and artificial neural network (ANN) in modelling of waste coconut oil ethyl esters production. *Energy Sources, Part A: Recovery, Utilization, and Environmental Effects*, *41*(9): 1049-1061, 2019.
18. Ebrahimpour, A., Rahman, R.N.Z.R.A., Ean Ch'ng, D.H., Basri, M. and Salleh, A.B. A modeling study by response surface methodology and artificial neural network on culture parameters optimization for thermostable lipase production from a newly isolated thermophilic Geobacillus sp. strain ARM. *BMC biotechnology*, *8*: 1-15, 2008.
19. Baş, D. and Boyacı, İ.H. Modeling and optimization I: Usability of response surface methodology. *Journal of food engineering*, *78*(3): 836-845, 2007.
20. Cai, J., Xu, D., Dong, Z., Yu, X., Yang, Y., Banks, S.W. and Bridgwater, A.V. Processing thermogravimetric analysis data for isoconversional kinetic analysis of lignocellulosic biomass pyrolysis: Case study of corn stalk. *Renewable and Sustainable Energy Reviews*, *82:* 2705-2715, 2018.
21. Vyazovkin, S., Burnham, A.K., Criado, J.M., Pérez-Maqueda, L.A., Popescu, C. and Sbirrazzuoli, N. ICTAC Kinetics Committee recommendations for performing kinetic computations on thermal analysis data. *Thermochimica acta*, *520*(1-2): 1-19, 2011.

22. Carrier, M., Auret, L., Bridgwater, A., and Knoetze J.H. Using apparent activation energy as a reactivity criterion for biomass pyrolysis. *Energy Fuels* 30: 7834-7831, 2016.
23. Yan, H.X., Hou, F.F., Zhao, H., Wang, H.N., Gao, S., Wu, M., Yu, P.Y., Liu, J.F., Li, N., Sun, Y.W. and Jiang, W. Pyrolysis kinetics of invasive coastal plant *Spartina anglica* using thermogravimetric analysis. *Energy Sources, Part A: Recovery, Utilization, and Environmental Effects*, *38*(19): 2867-2875, 2016.
24. Friedman, H.L. Kinetics of thermal degradation of char-forming plastics from thermogravimetry. Application to a phenolic plastic. In *Journal of polymer science part C: polymer symposia* (Vol. 6, No. 1, pages 183-195), 1964. New York: Wiley Subscription Services, Inc., A Wiley Company.
25. Akahira, T.J.R.R.C.I.T. and Sunose, T. Method of determining activation deterioration constant of electrical insulating materials. *Res Rep Chiba Inst Technol (Sci Technol)*, *16*: 22-31, 1971.
26. Flynn, J.H. and Wall, L.A. General treatment of the thermogravimetry of polymers. *Journal of Research of the National Bureau of Standards. Section A, Physics and chemistry*, *70*(6): 487, 1966.
27. Miura, K. and Maki, T. A simple method for estimating f (E) and k 0 (E) in the distributed activation energy model. *Energy & Fuels*, *12*(5): 864-869, 1998.
28. Vichaphund, S., Aht-Ong, D., Sricharoenchaikul, V. and Atong, D. Effect of CV-ZSM-5, Ni-ZSM-5 and FA-ZSM-5 catalysts for selective aromatic formation from pyrolytic vapors of rubber wastes. *Journal of Analytical and Applied Pyrolysis*, *124*: 733-741, 2017.
29. Wang, L., Lei, H., Liu, J. and Bu, Q. Thermal decomposition behavior and kinetics for pyrolysis and catalytic pyrolysis of Douglas fir. *RSC advances*, *8*(4): 2196-2202, 2018.
30. Kim, P., Johnson, A., Edmunds, C. W., Radosevich, M., Vogt, F., Rials, T. G., and Labbé, N. Surface functionality and carbon structures in lignocellulosic-derived biochars produced by fast pyrolysis. *Energy & fuels*, 25(10): 4693-4703, 2011
31. Rojas-Sandoval, J., *Tithonia diversifolia* (Mexican sunflower), Cabi compendium, Retrieved on 15/09/2018. https://www.cabidigitallibrary.org/doi/10.1079/cabicompendium.54020.